Extreme dimensional stability thermal control test

Thomas E. Brooks*[a], H. Philip Stahl[a]
[a] NASA's Marshall Space Flight Center, AL 35812;

ABSTRACT

Two observatories under consideration in the 2020 decadal survey include coronagraphs for characterizing the atmospheric composition of exoplanets. The telescope in those observatories must provide a wavefront that is stable to the picometer level for the coronagraph to provide enough starlight rejection to capture light reflected off of an Earth-like exoplanet. Therefore, picometer dimensional stability and control are required for these missions. Analysis indicates the thermal environment around the primary mirror must be stable to milliKelvin for the primary mirror's thermally induced wavefront error to be stable to picometers. Marshall Space Flight Center (MSFC) partnered with L3-Harris Corporation to design and build a 1.5m thermal control system capable of milliKelvin stability. MSFC tested this thermal control system in the X-Ray and Cryogenic Facility's large chamber to characterize how well the system controlled a 1.5m ULE® mirror.

Keywords: optothermal stability, thermal stability, thermal expansion, optomechanics, thermal control, HabEx, LUVOIR

1 Introduction

Two high-profile telescope conceptual designs, HabEx and LUVOIR, require wavefront stability on the order of 10pm/10 minutes. The required optothermal stability is likely to be even smaller than that. Analysis indicates that the primary mirror's environment must be stable to the mK level for the mirror to be thermally stable enough to meet these stringent optical stability requirements.[1] Optothermal testing has recently been performed in the X-ray and Cryogenic Facility (XRCF) to investigate how well a multizonal thermal control system can provide thermal stability to a 1-5m ULE® mirror. The results are contained in this paper.

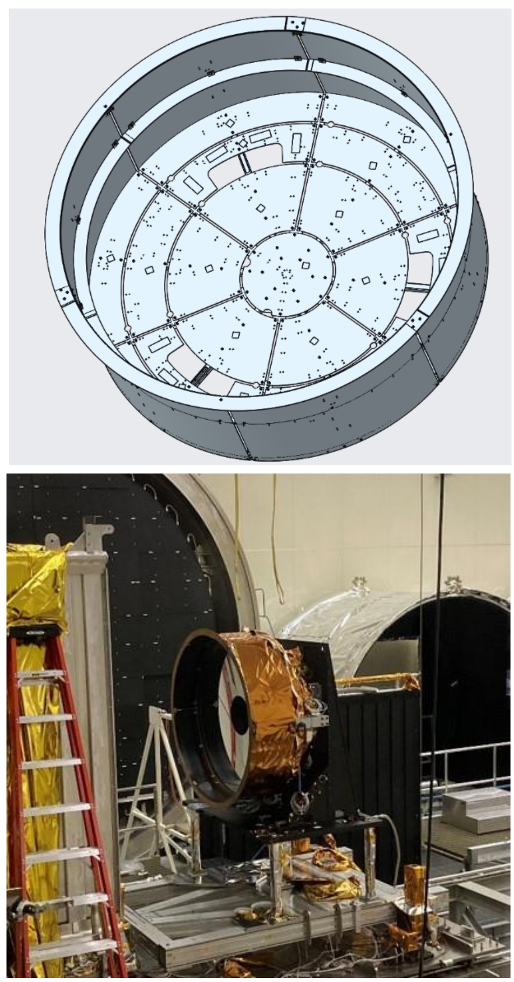

Figure 1: Top: CAD View of Mirror Heater Assembly. Bottom: MHA and mounted mirror on the test stand

2 Mirror Heater Assembly Design

The thermal control system, called the Mirror Heater Assembly (MHA), consists of 25 control zones arranged with cylindrical symmetry behind and around the sides of a mirror as shown in Figure 1. A 26th control zone maintains the temperature of the mirror's backplane. This thermal control system was sized to fit around a 1.5m mirror with a hexapod mount.

Platinum RTD (PT-100) sensors are bonded with stycast epoxy to roughly the center of every control zone, and heaters capable of operating at 100V (the maximum voltage before creating concerns of corona discharge in vacuum) were taped to the control zones with an acrylic

*thomas.brooks@nasa.gov; (256)544-5596 nasa.gov
2021 SPIE Optical Engineering + Applications (OP210); Paper 11819-9

adhesive. Silicon strain relief was removed to prevent potential off-gassing. The maximum required heater power was determined based upon thermal analysis of the test setup. A data acquisition system with an integral 22-bit digital multimeter was used to measure temperature to the nearest 1mK, and solid state relays pulse-width-modulated the power supplied to the heaters to provide proportional power. The 1mK precision of the DAQ limited the measured and the controllability provided by the thermal control system.

Control zones were black anodized and the outer surfaces of the MHA were generally covered in single-layer insulation. The two control zones nearest to the heat lamps were not covered in insulation in order to make it possible to produce a large thermal response with minimal heat, so that the test facility's environment (provided by a refrigeration system) would be as stable as possible. More insulation would be better for flight applications, but not for this stability testing, because the anticipated stability is already marginally measurable.

3 Test Setup

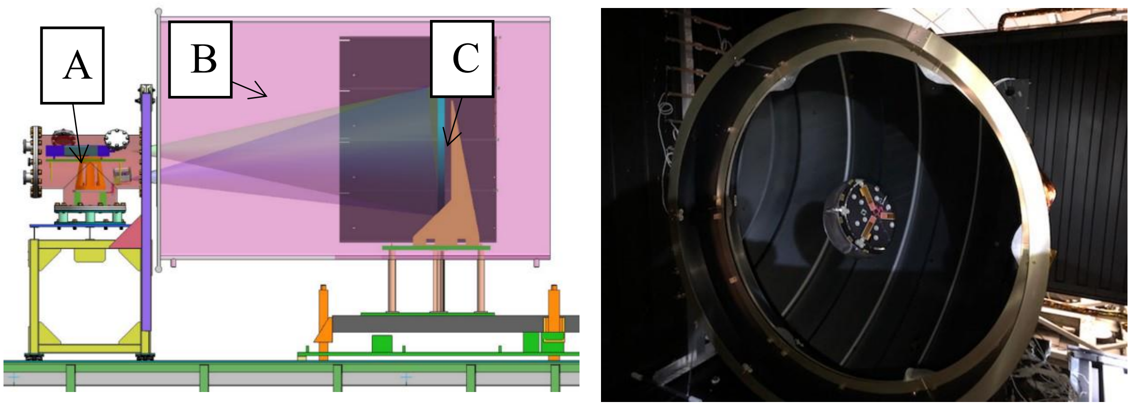

Figure 3: Left: Test Layout showing the interferometer (A), the inner shroud (B), and the mirror (C). Note that this figure does not include the Mirror Heater Assembly. Right: Mirror and MHA with the heat lamp array on the left side.

The test setup was as shown in Figure 3. The thermal control system was integrated around the hexapod-mounted mirror then mounted to the test stand. The test stand was moved on its rail into the inner shroud. Thermal control and telemetry cabling was fed through the chamber walls and read by two data acquisition systems. A heat lamp array was placed next to the test article.

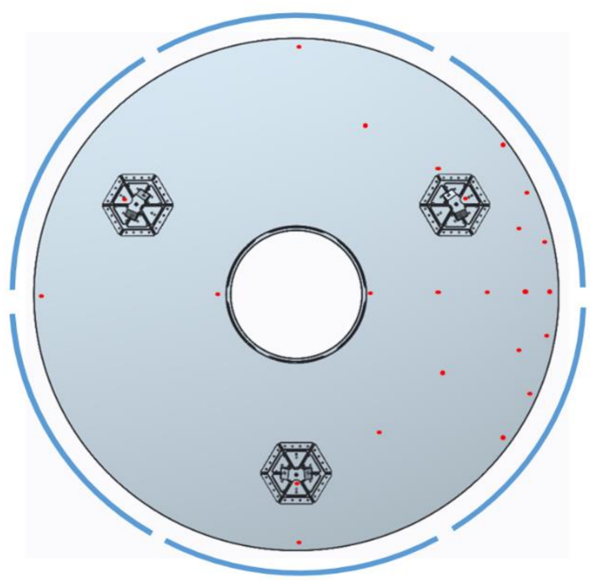

Figure 2: Thermal Diode Sensor Locations (red, on mirror), control zones (blue, around mirror), and heat lamp array (blue, to the right of the mirror).

The test mirror's surface is a sphere which minimizes the potential for alignment-induced measurement error. An interferometer was aligned to the mirror to measure changes in its surface figure, and a measurement was taken in ambient air. The entire chamber was evacuated, and another surface measurement was taken and found to have changed little from the ambient measurement. The inner shroud was cooled to

~225K (-47 ˚C) using liquid nitrogen to provide a powerful heat sink that cold biases the system and increases the maximum thermal disturbance that may be applied by the heat lamps.

Pre-test thermal analysis estimated the temperature gradient that would occur during the test. This a priori temperature gradient was used to locate temperature sensors in positions which would provide the best knowledge of the gradients. The temperature sensor locations, heater zones, and the heat lamp array are shown in Figure 2.

The difference between back-to-back surface figure measurements was routinely <2 nm root-mean-squared (RMS) when using the average of 128 phase measurements as shown in Figure 4. This <2 nm error is largely attributable to vibrations produced by cryogen and vacuum pumps. A slow drift in pixel readings also occurred at a rate of approximately 1nm per 6 hours. This drift created a random static error which is alien to any mechanical disturbance (these usually manifest in low-order Zernike shapes). Even with the low noise floor in the surface measurements, the temperature sensing system proved to be orders of magnitude more sensitive to thermal disturbances than the interferometer. Therefore, in a flight system, after the coronagraph has established a dark-hole, maybe the control system should use thermal sensors to maintain the dark-hole.

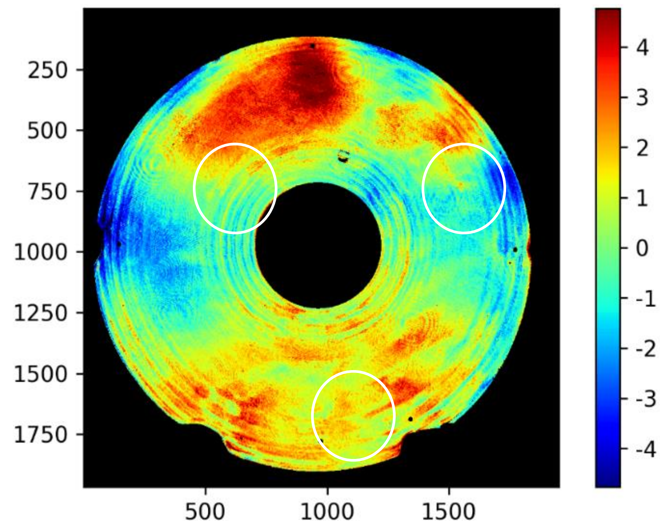

Figure 4: Periodically, two back-to-back measurements were taken and subtracted to find the measurement repeatability. This image is an example of the repeatability measurement. The RMS of this repeatability is 1.6nm. Approximate mount locations are circled in white.

4 Pre-test Experiments

Before the vacuum chamber was evacuated, the control system parameters were tuned with the control zones in air. After the chamber was evacuated and before testing began, the control system parameters were tuned for the vacuum chamber environment. During this process, there were long periods of time with minimal external disturbance, so the thermal stability of the MHA in a low-disturbance environment was observed.

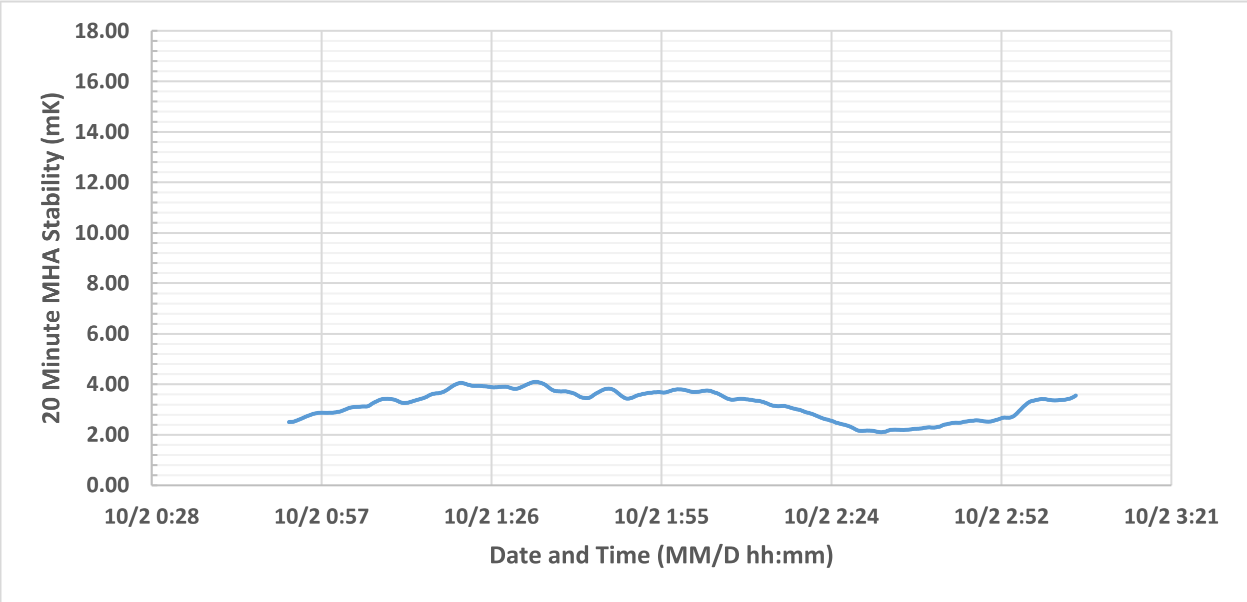

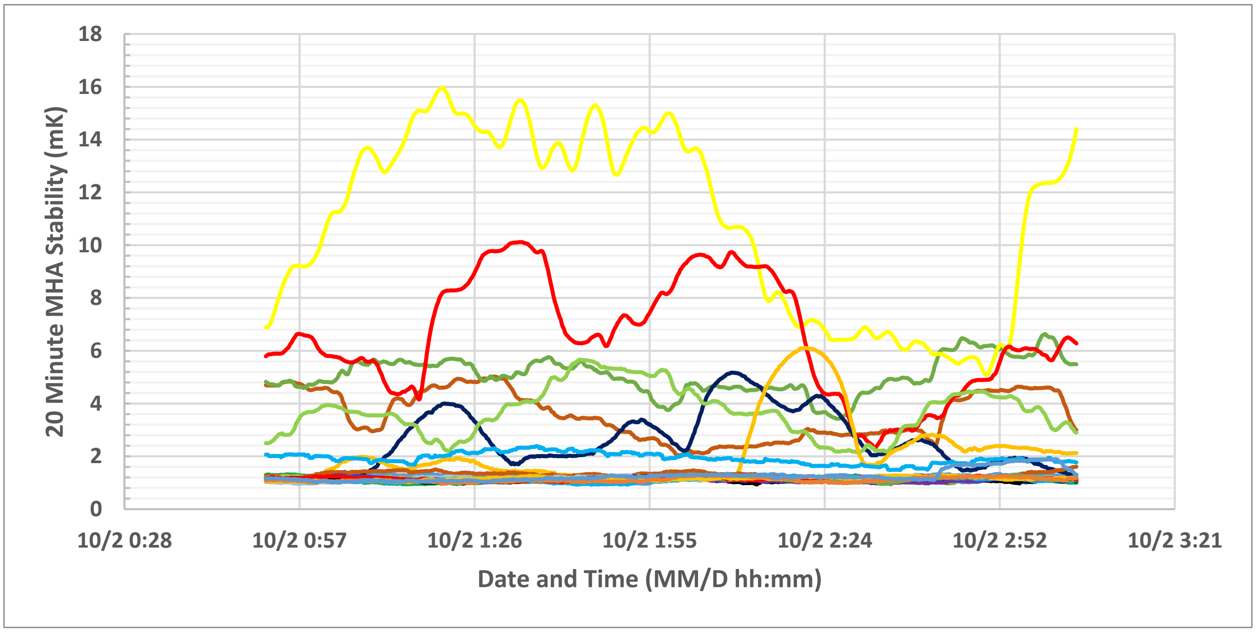

Figure 5: The top graph shows the RMS stability of all of the zones, and the bottom graph shows the standard deviation (over 20 minutes) of every zone.

The standard deviation of most of the zones over the preceding 20 minutes were below 2mK as shown in the bottom graph in Figure 5. The top graph shows the RMS of all the standard deviations at every moment in time. If more labor is allocated for tuning the controller, it is expected that these few relatively unstable zones (16 mK) would reach sub-2mK performance like the other zones. Other approaches for increasing the system's stability are addressed in section 7.

5 Heat Lamp Disturbance Test

The objective of the Heat Lamp Disturbance Test was to determine how well the MHA could negate the effect of a thermal disturbance (in this case, the heat lamps) on the 1.5m ULE mirror. The Heat Lamp Disturbance Test involves the following steps: 1) the MHA was turned on and run overnight to reach stability, 2) the heat lamp array was turned on to a total of 360VA of 3-phase power to create a thermal disturbance, 3) after stability was reached, the heat lamp array power was increased to 720VA 3-phase, 4) finally, the heat lamps were turned off. This sequence was repeated twice – once with active control and again with constant MHA heater power - to compare the effect of the heat lamps when the mirror is passively controlled with their effect when the MHA actively negates the heat lamp's effect.

5.1 SFE Results

The mirror's figure never changed by a discernable amount during active control. The mirror's surface did change by 5nm RMS as shown in Figure 6 during the passive test. The SFE measurement shows astigmatism and the bond pad effect (the puckering on the top left bond-pad). Active control performed better, but we could not tell from direct SFE measurement how much better it performed, because the heat lamp effect during active control was less than the 2nm repeatability of SFE measurements. The level of performance gain from active control can be indirectly observed from temperature measurements.

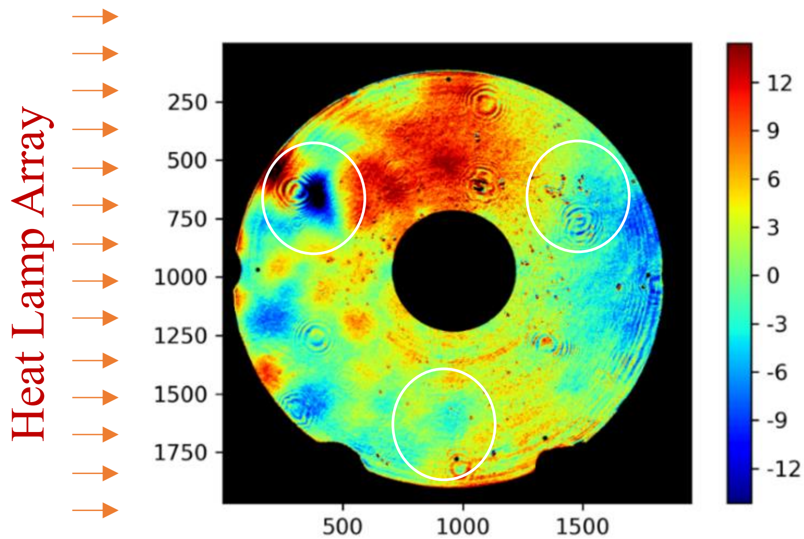

Figure 6: Change in SFE caused by 720VA with Constant Heater Power (the passive case). The approximate mount locations are identified with the white circles

5.2 Temperature Results

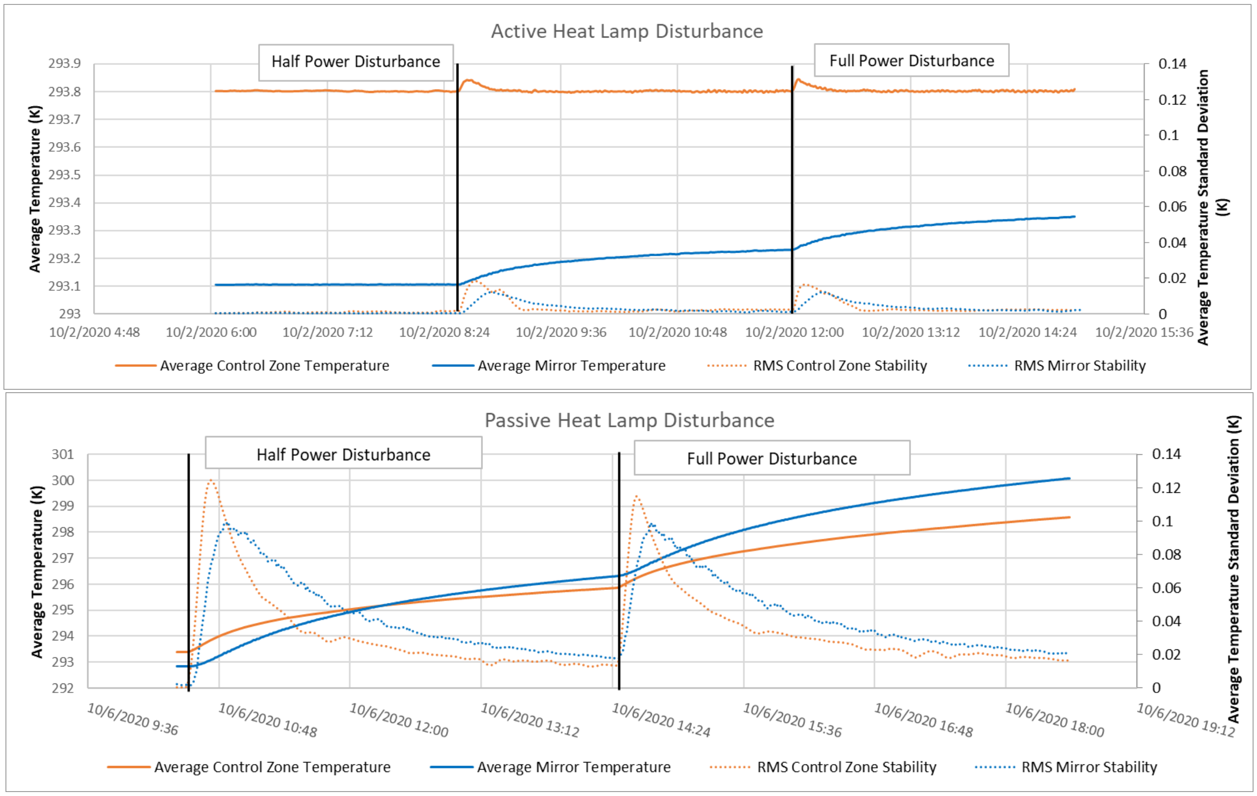

Figure 7: Heat Lamp Disturbance with Active Control (top) and without active control (bottom)

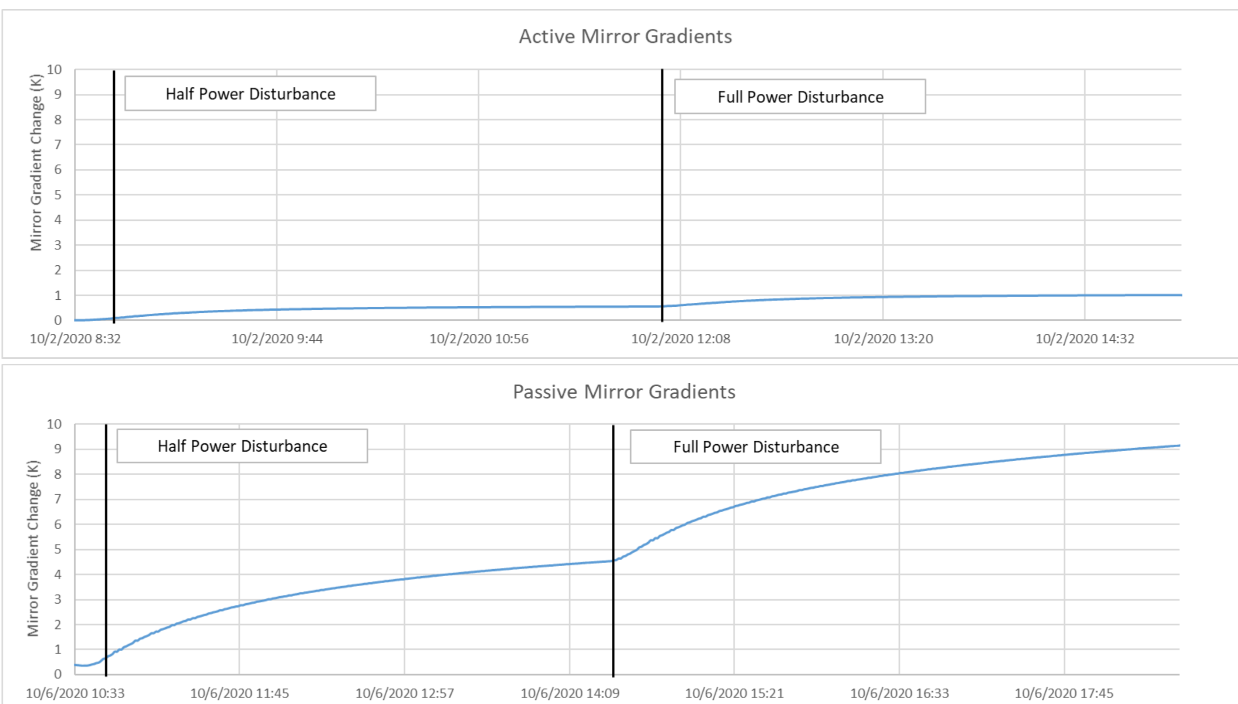

Figure 8: Mirror Gradient Changes during Active and Passive Control

The temperature results during the active and passive portions of the test are shown in Figure 7 for comparison. The average mirror temperature changed by 250mK under active control and 7220mK (29x greater) under passive control. The control zones had a maximum instability that was 6x less during active control than during passive control, and returned to full stability after 30 minutes, while the passive case never reached that stability during the 4 hours they were given. This data only considers the average temperatures of the mirror and the zones.

Figure 8 shows how the gradients in the mirror changed over time. The y axis in Figure 8 is described in the equation below where Δ_t is the Mirror Gradient Change at time t, N is the number of sensors on the mirror (24 in this case), $T_{i,t}$ is the temperature at sensor i and time t, and $T_{i,0}$ is the temperature at sensor i before the start of the test:

$$\Delta_t = \left(\frac{\sum_{i=0}^{N} (T_{i,t} - T_{i,0})^2}{N} \right)^{0.5}$$

The 720VA heat lamp thermal disturbance is roughly equivalent to 8,000 times greater than if HabEx's baffle were to change its temperature by 50mK (a reasonable amount).

The thermal stability around a HabEx mirror was previously defined as a function of the period of the temperature fluctuations.[2][3] A Fourier transform was performed on test data to consider the stability in the time domain. Frequency was converted to period to match the previous analysis. A comparison between the test results and the HabEx requirement is in Figure 9. Note that the test has a disturbance that is 8000x greater than if a telescope's baffle changes in temperature by 25mK (a notional flight-like disturbance), and the control system is for a 1.5m mirror (HabEx is 4m). The gray HabEx requirement line indicates that the mirror will not maintain stability if a single disturbance exists above and to the right of the line. It does not consider the summation of multiple disturbances existing simultaneously. Further analysis will more exactly compare the test results to the HabEx requirement, but these findings are encouraging.

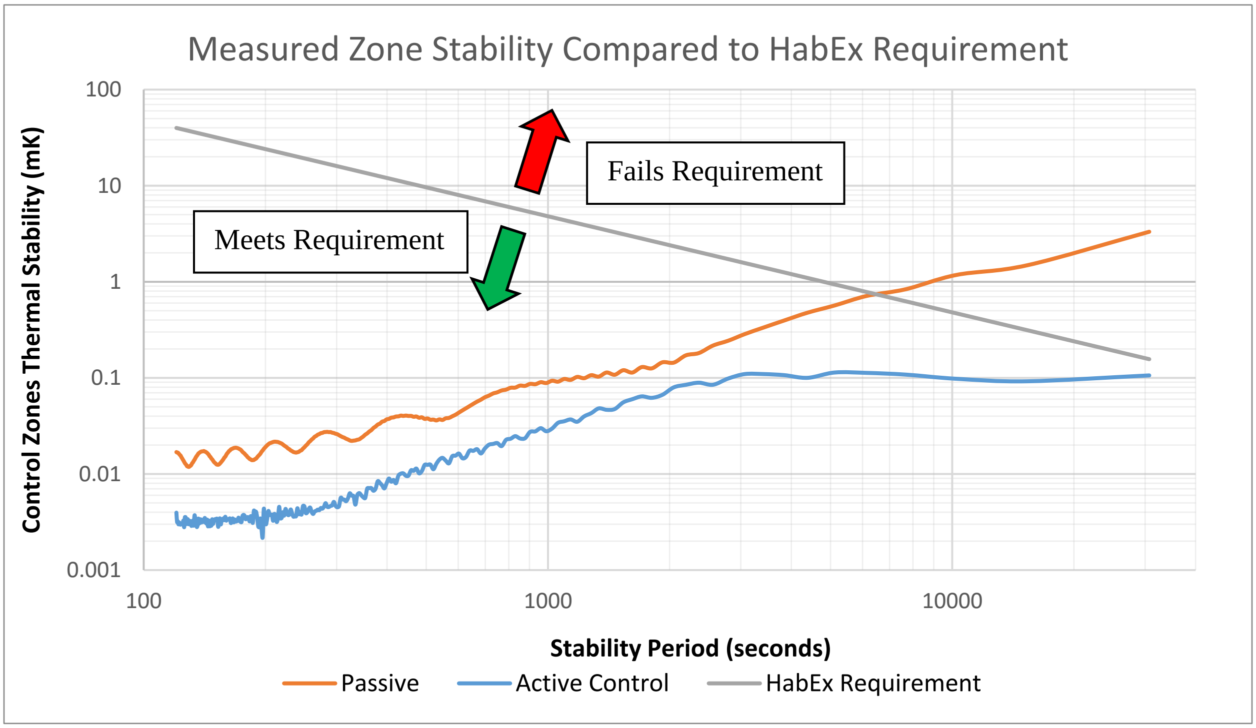

Figure 9: Measured thermal stability for the passive and active heat lamp thermal disturbance test compared to an established HabEx stability requirement.

6.1 Astigmatism

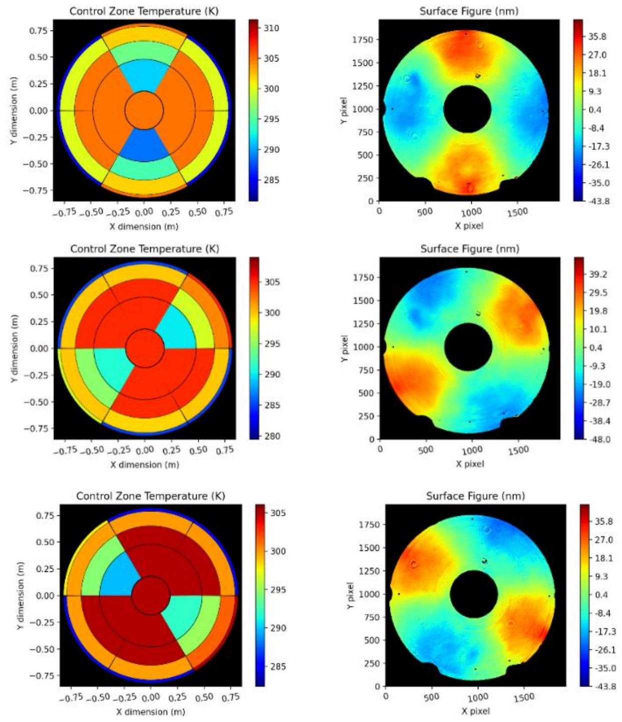

Figure 10: Left: Control Zone Temperatures. Right: Surface Figure.

Astigmatism is an extremely common mechanical surface figure error, because a disk shape is predisposed to bend astigmatically due to its stiffness distribution. The amplitude of astigmatism in a mirror is always incidentally affected by the temperature and CTE distribution in a mirror, but in this test the thermal state was intentionally used to control the astigmatism in the mirror. Analysis from previous work discovered the sensitivity of a mirror's astigmatic response to a given temperature distribution to be greatest when the temperature distribution is a high-order astigmatism with multiple radial lobes.[1]

For this reason, the control zones were set to the temperatures shown in Figure 10 which resulted in the surface figures shown in the same figure. We could produce the astigmatic response every 60 degrees. The surface changed by 16nm RMS as a result of the 30K temperature distribution in the MHA. The mirror has a sensitivity to this temperature distribution of 0.53nm/K. Video was produced and released that shows the change in SFE and Control Zone Temperature over time, and that video is available in the presentation that accompanies this paper.

6.2 Trefoil

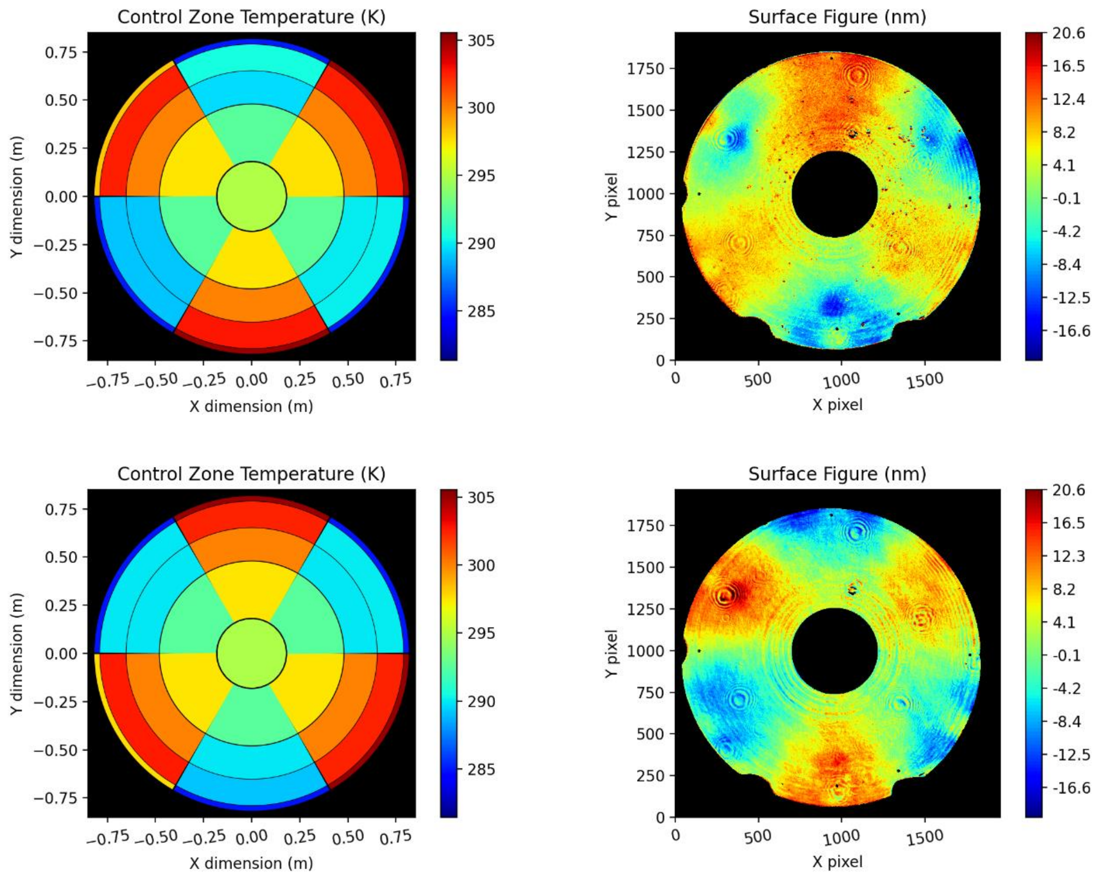

Figure 11: The left side shows the temperature distribution in the MHA in Kelvin, and the right side shows how much the mirror's surface changed in nanometers. This data is at a thermal steady state condition.

Trefoil is a relevant Zernike, because it is often caused by a mirror's mount. Also, some coronagraphs are sensitive to trefoil.[4][5][6] In our tests, we intentional induced trefoil by changing the temperature distribution in the control zones. The 6Θ symmetry of the MHA makes it possible to produce only one phase of trefoil at positive and negative amplitude. The two temperature distributions and their resulting SFEs are shown in Figure 11. The 25K gradient in the control zones produced a 7nm RMS shape change in the mirror, so the mirror had a 0.28nm/K sensitivity to this temperature distribution. If looking at this from the view of an actuator, we'd want that sensitivity number to be large, but if looking at it from the perspective of thermal stability, we'd want that sensitivity number to be small.

6.3 Coma

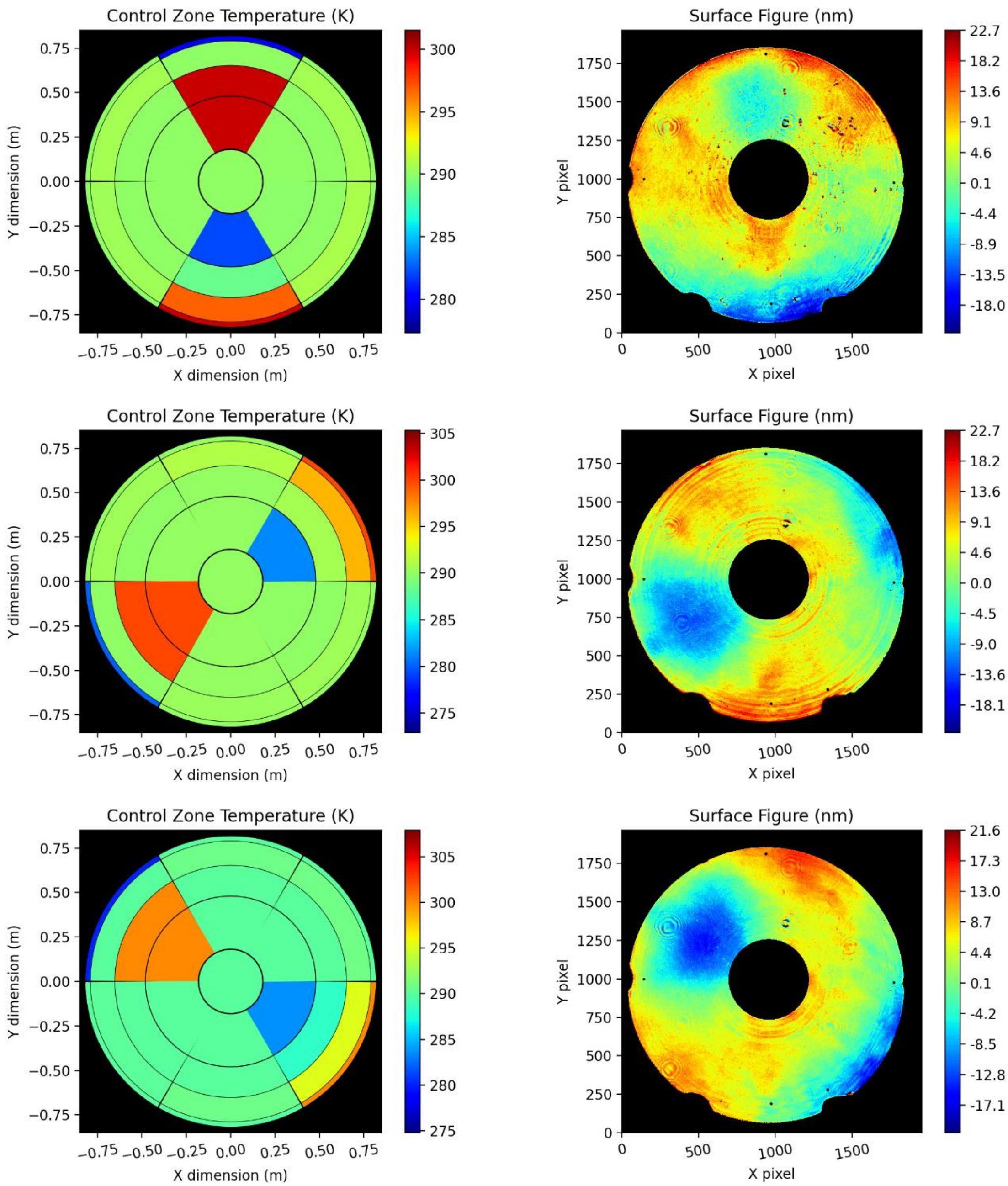

Figure 12: The left shows the temperature distribution in the MHA and the right shows the resulting change in the mirror's surface.

Coma is another common surface figure that is typically caused by a lateral temperature gradient (for example, sunlight heating the side of the telescope baffle) or a decentering of the telescope's secondary mirror. The MHA symmetry allowed for 6 phases (every 60 degrees) of a Coma-like signature to be produced. The 34K gradient in the MHA produced a 6.8 nm RMS change in the surface figure, so the mirror has a 0.2nm/K sensitivity to this temperature distribution.

6.4 Linearity of Temperature Distributions

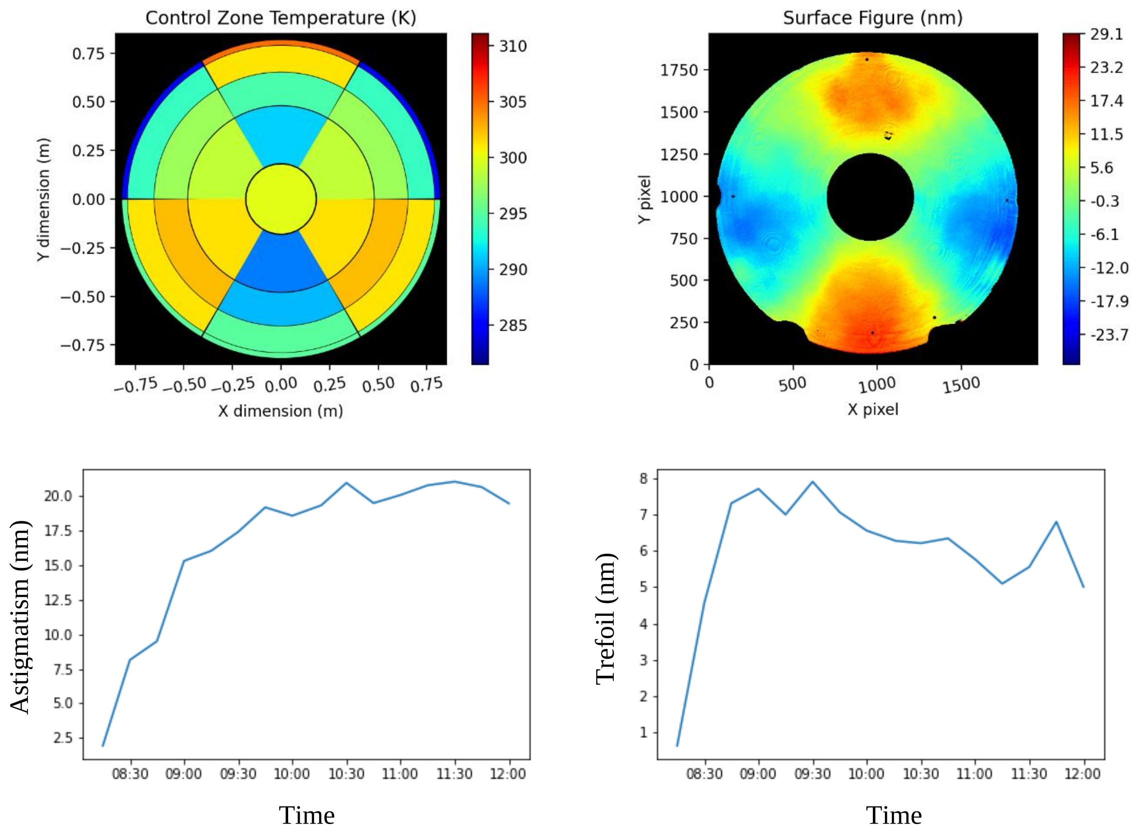

Figure 13: The top shows the MHA's temperature distribution and the resulting change in surface. The bottom shows the change in the mirror's Astigmatism and Trefoil coefficients of the duration of the test.

It is important to understand the linearity of the relationship between the temperature distribution and the change in surface, so that it's possible to easily extrapolate from these results. A test was performed to discover if the combination of two temperature gradients would result in the combination of their two resulting surfaces.

The astigmatic temperature distribution was expected to produce 18nm of astigmatism, and the trefoil temperature distribution was expected to produce 7nm of trefoil. Because the Zernike coefficients from the test were 20nm for astigmatism and 6.5nm for trefoil, this test produced astigmatism and trefoil in amounts that prove linearity sufficiently well for it to be a good rule of thumb.

7 Future improvements

The MHA provided excellent performance in the areas which we intended to test, but there are still clear paths to further improve performance. The paths to increased performance are covered in the following sections.

7.1 Increase the heat capacitance of the control zones

Zones with greater heat capacitance have a longer time constant, and their temperature will change slower than zones with a lesser heat capacitance. Zones with higher heat capacitance will change temperature less between control cycles. Therefore, increasing heat capacitance will result in improved stability as was observed when comparing the zones in region 3 (shown in Figure 14).

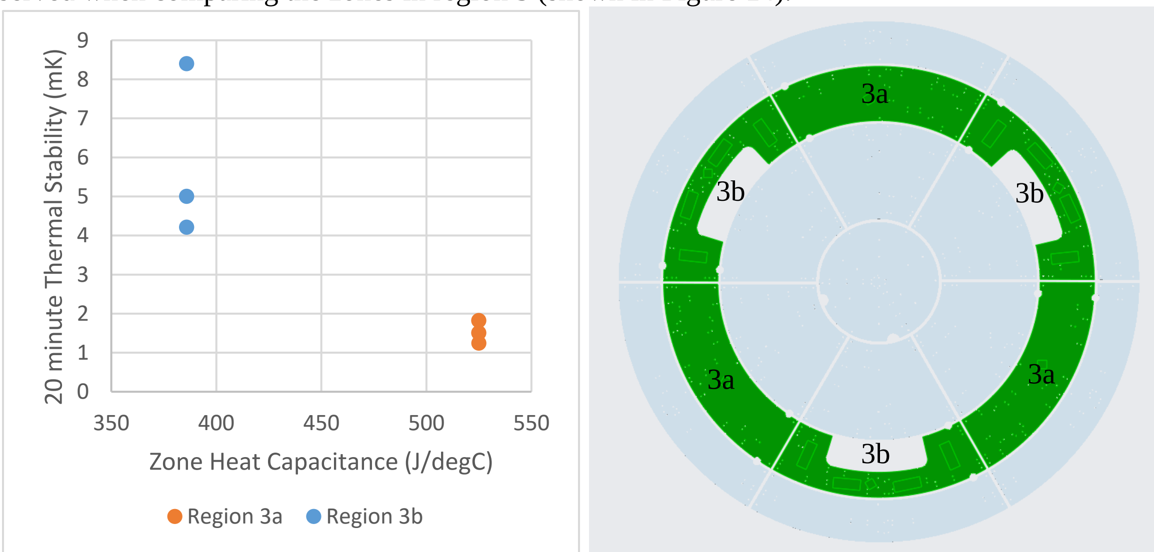

Figure 14: Left: The thermal stability during the heat lamp test. Right: A CAD Rendering of Region 3. Region 3 is subdivided into regions 3a and 3b, because some of the zones have cutouts for the hexapod struts. 3a and 3b experience similar thermal disturbances but yielded different thermal stabilities due to differences in heat capacitance.

The comparison between region 3a and 3b is particular apt, because they are at similar locations, so the only difference is their shape. This general trend was observed between other regions as well.

7.2 Increase the conductance in the control zones

The measured temperature stability reached ~2mK during these tests, but temperature gradients in the zone around the sensor were likely changing by a significantly greater amount. If the zone had a higher conductance by using a more conductive material, a larger thickness sheet, or some novel approach, the thermal control zones would be more isothermal and effectively more stable.

7.3 Increase the insulation around the control zones

More insulation around the control zones would reduce the magnitude of an external thermal disturbance. This would have been counterproductive to our overdrive test but would be beneficial for a flight system. Using MLI (rather than the SLI we used) will improve the isothermality of the control zones, so long as the heaters provide heat homogenously.

7.4 Increase uniformity of the heat provided to the control zones

Mass produced heater tape was used for this experiment, so the heater tape did not heat ever section of the control zones an equal extent. There are commercially available options for making custom heater tape shapes, and custom heaters can provide greater heating homogeneity which will result in lower-order temperature gradients in the mirror and less thermally induced SFE.

7.5 Increase the number of bits in the DMM used to measure temperature

Our data acquisition system used a 22-bit DMM which gave us a measurement precision of 1mK. The high-time-constant heater zones had a stability which was limited by this 1mK measurement precision, so the thermal stability of those control zones was ultimately limited by the DMM. It is easily within reach of current technology to produce DMMs with more bits, and that would certainly improve a future control system.

7.6 Better sensor attachment

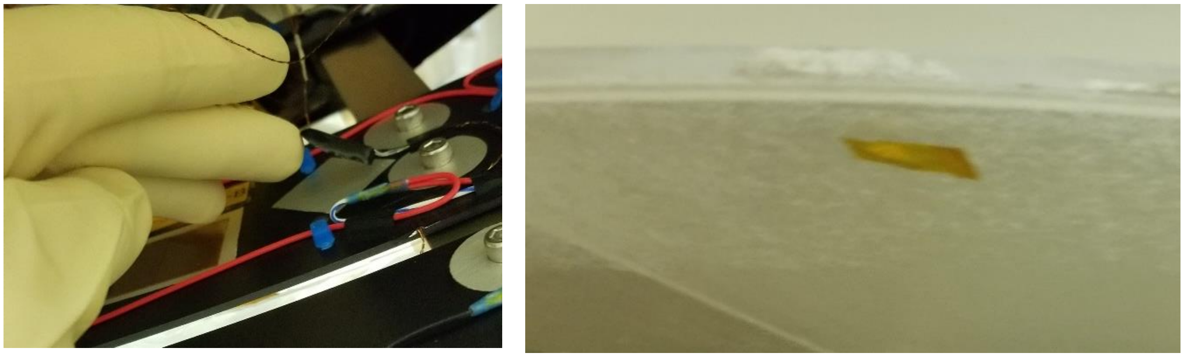

Figure 15: At left is a sensor that was attached to an aluminum control zone with stycast, and at right is a piece of Kapton tape which originally had a sensor under it.

Sensors were attached to the mirror using Kapton tape, and they were attached to the control zones using a stycast epoxy. Two of the 26 sensors debonded from their control zone at an unknown time (presumably during the test). The sensors experienced temperatures ranging from 245 and 315K. Most likely, the bond failed due to a thermal stress. Sensor lugs or an imbedded sensor bonded with conductive epoxy are two options for improvement.

The sensors adhered with Kapton to the mirror did not experience as wide of a temperature range, but one sensor completely fell off the mirror, and a second sensor is only loosely attached to the mirror. The cause of this is unknown but thought to be from strain occurring between the tape and the strain relief.

8 Conclusion

A multizonal Mirror Heater Assembly (MHA) was tested to thermal loads that were significantly larger than what would be experienced on orbit. The tests proved that a thermal control system with this architecture is capable of controlling optics to the levels required by HabEx. Several paths to further improve performance are also provided.

The testing also measured the sensitivity of the mirror to certain temperature distributions in the MHA and found that linear superposition of temperature distributions produces their superimposed changes in surfaces. This fact is very useful for modelling purposes. These sensitivities can be compared to flight analyses to ensure that the mirror meets optothermal stability requirements.

9 References

[1] Thomas E. Brooks, Ron Eng, Tony Hull, and H. Philip Stahl "Modeling the Extremely Lightweight Zerodur Mirror (ELZM) thermal soak test", Proc. SPIE 10374, Optical Modeling and Performance Predictions IX, 103740E (6 September 2017); https://doi.org/10.1117/12.2274084

[2] Brooks, Thomas, H. Philip Stahl, William R. Arnold, "Advanced Mirror Technology Development (AMTD) thermal trade studies", Proc. SPIE 9577, Optical Modeling and Performance Predictions VII, 957703 (23 September 2015); doi: 10.1117/12.2188371; https://doi.org/10.1117/12.2188371

[3] Brooks, Thomas E, "Predictive thermal control applied to HabEx", Proc. SPIE 10398, UV/Optical/IR Space Telescopes and Instruments: Innovative Technologies and Concepts VIII, 1039814 (5 Sept 2017); doi: 10.1117/12.2274338; https://doi.org/10.1117/12.2274338

[4] J. J. Green and S. B. Shaklan, "Optimizing coronagraph designs to minimize their contrast sensitivity to low-order optical aberrations," in Technical and Instrumentation for Detection of Exoplanets, *SPIE* **5170**, 25 (2003)0 [doi: https://doi.org/10.1117/12.506485].

[5] D. Mawet et al., "The Vector Vortex Coronagraph: sensitivity to central obscuration, low-order aberrations, chromaticism, and polarization," in *Modern Technologies in. Space- Ground-based Telescopes and Instrumentation*, *SPIE* **7739** (2010) [doi: https://doi.org/10.1117/12.858240].

[6] Nemati, Bijan, H. Philip Stahl, Mark T. Stahl, Garreth J. Ruane, Leah J. Sheldon, "Method for deriving optical telescope performance specifications for Earth-detecting coronagraphs," J. Astron. Telesc. Instrum. Syst. 6(3), 039002 (2020), doi: 10.1117/1.JATIS.6.3.039002.